Amphiphilic Self-Assemblies Decorated by Nucleobases

Debora Berti,* Francesca Baldelli Bombelli, Martina Fortini, and Piero Baglioni*

Department of Chemistry and CSGI, University of Florence, Via della Lastrucccia 3-Sesto Fiorentino, Florence, 50019, Italy

Received: June 7, 2007; In Final Form: July 18, 2007

Phosphatidyl-nucleosides are a class of functional amphiphiles, where a nucleic acid monomer is conjugated to a lipid skeleton. These derivatives self-organize in aqueous solution as assemblies of various size, shape, and interfacial curvature. This paper presents a comparison of the aggregation behavior of different 1-*R*,2-*R*-*sn*-glycero-3-phosphatidyl-nucleosides, where R = 8 (DiC_8PN) or R = 12 (DLPN) and N is either adenosine (a purine) or uridine (a pyrimidine), a complementary pair in RNA. Surface tension, small angle neutron scattering, cryo-TEM, and circular dichroism are used to highlight and distinguish the impact of the hydrophobic assembler and of the base substitution on the solution phase behavior. Our main conclusion is that the nucleic functionalization provides an additional parameter to control self-assembly through specific interactions among the polar heads. Further nonideal effects are induced by mixing nucleolipids with complementary base substitution. We show that these contributions alter the aggregation thresholds and modulate properties of the aggregates on the mesoscale.

Introduction

Amphiphilic self-assembly represents the noncovalent alternative to supramolecular "bottom-up" engineering of artificial nanostructure devices. The advantage over conventional covalent molecular architectures lies mainly in the stimuli-responsive character, in the thermodynamic control of the size and shape of the obtained nanostructures (and therefore in their reversibility), and in the generally easy and low-energy consumption preparation. The typical independent parameters of the phase diagram are surfactant volume fraction, temperature, and ionic strength: subtle variations of local microstructure can lead to cascade effects with dramatic morphological transitions on the mesoscale.[1] This flexibility can be further enhanced and enriched by chemical design of the molecular building blocks: this route has led to the relatively new field of functional surfactants, where an additional control parameter (i.e., photosensitivity,[2] redox activity,[3] etc.) is chemically encoded in the amphiphile.[4] The ability to exploit the self-organization of functional assembling molecular building blocks and the possibility to impart tunable, responsive properties on the resulting aggregates has led to a dramatic growth in the activity and understanding of this area. Peptide-amphiphiles and oligonucleotide-amphiphiles[5,6] represent one of the most interesting and recent examples in such a field. The practical application of such bottom-up assemblies in supramolecular or biomedical fields requires the ability to synthesize molecules in a highly controlled fashion and to predict the microstructure of the aggregate.

We are interested in the self-assembly of nucleolipids[5] composed of nucleotides, the building blocks of nucleic acids,[7] covalently attached to a hydrophobic unit. The possibility to integrate such molecular functions into amphiphilic molecules and use the know-how of soft matter to engineer nano-objects with nucleic decoration, can ultimately lead to extremely complex and fascinating structures.[8−13]

The use of such self-assemblies opens new perspectives in the field of nanoscience. The digital pairing of oligonucleotides can be exploited for example to build hierarchically organized addressable architectures[14−16] with functional and positional control on the nanoscale.

In the past years several examples of bioinspired amphiphiles with nucleic functionalities have appeared in the literature.[17,18] Barthelemy et al.[19,20] reported the design and synthesis of a novel class of zwitterionic dialkyl-nucleophosphocholines and have introduced several chemical modifications either on the base or on the phosphocholine side, also changing the net charge of the molecule.[21] Shimizu's group synthesized nucleotide bolamphiphiles with water gelling ability, through the spontaneous formation of a fibrous network, and found a remarkable dependence of fiber morphology on the presence (and length) of complementary oligonucleotides.[22,23]

In 1987, Satoshi Shuto[24] and collaborators proposed a remarkably elegant one-pot technique to modify enzymatically phospholipids, exchanging the choline headgroup with a nucleoside. The reaction allows the use of natural building blocks and affords derivatives in reasonably good yields. The resulting derivative (phosphatidylnucleoside, PLN, shown in Scheme 1)[25] has a nucleotide block as polar head and reproduces the chemistry and the charge of a DNA monomer. The first morphological characterization of phosphatidylnucleosides bilayers was due to the group of Yanagawa.[26] Following their seminal papers, phosphatidylnucleosides aggregation and molecular recognition properties have been studied in some detail in the following years.

A coarse grained mapping of phosphatidylnucleoside phase behavior can be performed by comparison with the synthetic precursor phosphatidylcholines. Lecithins, one of the most important classes of phospholipids, are the major structural components of biological membranes, and their self-assembly in bilayer structures, formed by longer chain derivatives, has been the subject of classical studies in the past both from a structural and dynamic point of view.[27−29] Derivatives with acyl

* To whom correspondence should be addressed. E-mail: berti@csgi.unfi.it; baglioni@csgi.unifi.it..

10.1021/jp0744073 CCC: $37.00
Published on Web 09/19/2007

SCHEME 1: Sketch of the Chemical Structures of the Nucleolipids Investigated in This Study and Representation of Their Packing Hindrances in a Self-assembly; the Continuous Line Represents Interfacial Curvature

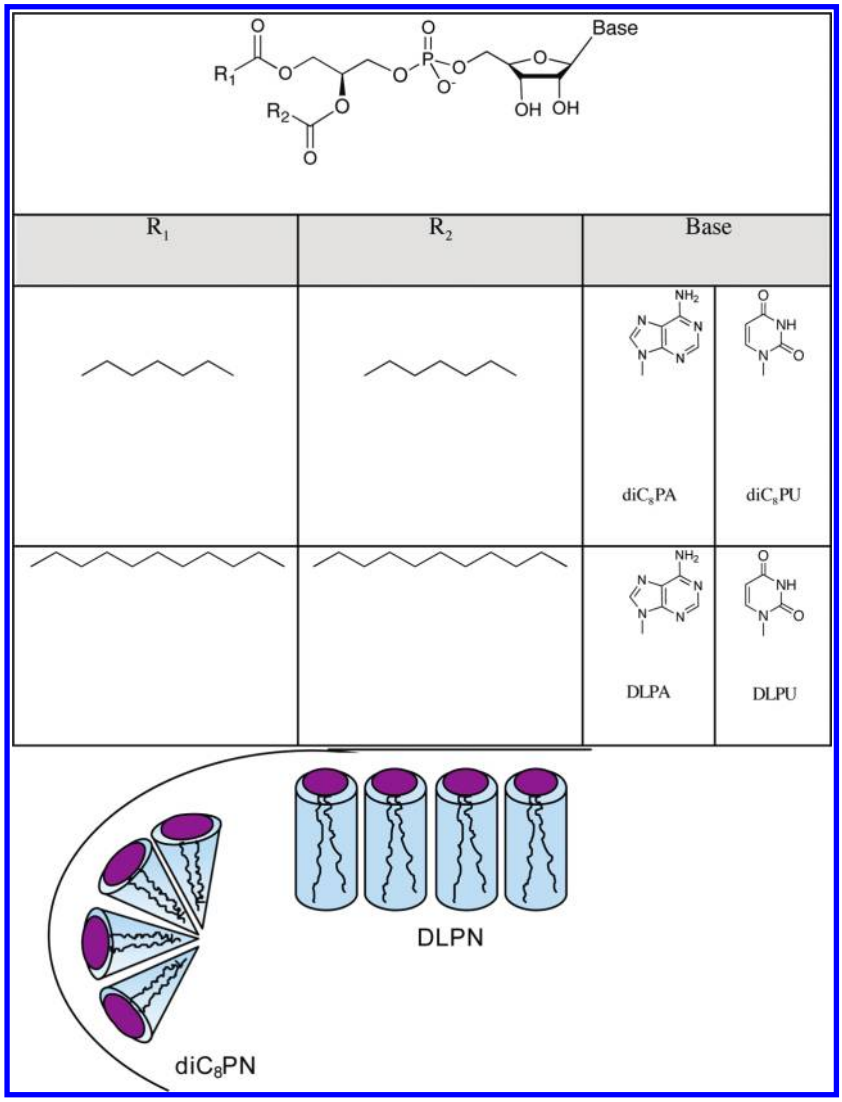

chain length ranging from six to nine are conventionally termed "short chain" lecithins.[30−32] The balance between the hydrophobic and the hydrophilic portions of these short chain zwitterionic phospholipids, according to the classical Ninham approach,[33] favors the existence of L_1 micellar phase, which has been extensively investigated as a model for the mechanism of action of phospholipases.[34,35] Some classical structural studies have also been performed on micellar growth of symmetric and asymmetric series of short chain lecithins, showing a consistent dependence on the fatty chain length.[36−39]

We expect that "long chain" phosphatidylnucleosides derivatives will exhibit self-assembly properties similar to the corresponding lecithins, while short chain compounds will display consistent differences, owing to the higher impact of the ionic polar-head substitution with respect to the overall structure of the surfactant. POPNs (1-palmitoyl, 2-oleoyl, phosphatidylnucleosides) organize into zero-curvature structures, like POPC.[25,40] Conversely diC_8PN-DLPN derivatives form micellar aggregates in aqueous solution.[41,42] Selective and preferential interactions have been identified between adenine and uracil moieties, according to a pattern resembling to the molecular recognition in nucleic acids.[41] Recently, it has been demonstrated that micellar aggregates template the formation of superstructures in the presence of complementary oligonucleotides.[43]

For micelles, the onset of aggregation, shape, and size are ruled by thermal equilibrium and can be altered through the variation of a control parameter. It is therefore interesting to highlight the different contributions of the hydrophobic part and of the nucleic motif to determine the final aggregate.

For this purpose we have designed and studied a set of nucleolipids differing in their hydrophobic chains, namely dioctanoyl-phosphatidyl-N (diC8PN) and dilauroyl-phosphatidyl-N (DLPN), with N either adenosine or uridine, whose structure is sketched in Scheme 1.

Surface tension, SANS, cryo-TEM, and spectroscopic methods are used in this study to compare the aggregation properties of these amphiphiles. The leading energetic term in determining the aggregate morphology is due to the hydrophobic assembler, but a fine-tuning can be introduced by a proper selection of the polar head. This latter contribution originates not only from electrostatic or excluded volume interactions, as in conventional surfactants, but also by the specific recognition properties between complementary bases.

Experimental Section

Materials. *1,2-Dioctanoyl-sn-glycero-3-phosphatidyl-nucleosides and 1,2-dilauroyl-sn-glycero-3-phosphatidyl-nucleosides.*

TABLE 1: Samples Investigated through SANS

concentration [mol/L]	volume fraction	sample name
	DiC_8P-Uridine (diC_8PU)	
1.0×10^{-1}	5.0×10^{-2}	A
7.5×10^{-2}	3.7×10^{-2}	B
5.0×10^{-2}	2.5×10^{-2}	C
3.0×10^{-2}	1.4×10^{-2}	D
1.0×10^{-2}	5.0×10^{-3}	E
	Dlp-Uridine (DLPU)	
1.0×10^{-1}	6.4×10^{-2}	A′
7.5×10^{-2}	4.8×10^{-2}	B′
5.0×10^{-2}	3.2×10^{-2}	C′
1.0×10^{-2}	6.4×10^{-3}	D′
7.5×10^{-3}	4.8×10^{-3}	E″
5.0×10^{-3}	3.2×10^{-4}	F′
2.0×10^{-3}	2.5×10^{-4}	G′
1.0×10^{-3}	6.4×10^{-5}	H′

diC_8PN and DLPN (with N either adenosine or uridine) were prepared by enzymatic trans-esterification of the corresponding phosphocholines in a chloroform/water system, as already reported.[40] DLPC and DiC_8PC were purchased from Avanti Polar Lipids (Alabaster, Alabama), while adenosine and uridine have been provided by Fluka, Switzerland. Phospholipase D from Streptomyces sp. was a generous gift from Asahi Kasei Corporation, Tokyo. After isolation of the nucleolipid from the byproducts, the purity of the final compounds was checked by TLC and NMR spectroscopy. All the reagents employed for the synthesis were of +99% purity grade. Micellar solutions were prepared by weighing the lyophilized powder, adding D_2O or phosphate buffer 0.1 M at pH = 7.5 (PBS) in D_2O, and stirring gently at room temperature until complete dissolution. The pH of D_2O was adjusted to 7.0 with NaOD concentrated solutions.

Methods. *Small Angle Neutron Scattering*. SANS experiments were performed at BENSC (Hahn Meitner Institut, Berlin, Germany) at the V4 spectrometer and at LLB (Saclay, France) at the PAXE instrument. D_2O was used as a solvent to enhance the neutron scattering contrast of apolar tails and to reduce the contribution of the incoherent scattering to the spectrum.

Data reduction to absolute intensities was performed according to experimental reduction protocols available at the experimental facilities.[44] The raw spectra were azimuthally averaged, corrected for background and cell contribution, and converted to absolute intensities using H_2O isotropic incoherent scattering as a reference, according to conventional procedures. The solvent and cell contributions were subtracted prior to data analysis. The samples investigated are summarized in Table 1.

Data Analysis. A correct interpretation of the experimental small-angle spectra in the concentration and ionic strength ranges under examination requires that both intraparticle and interparticle correlations are taken into account. Quantitative analysis of absolute scale SANS data was obtained by modeling the micellar solution as composed of charged core−shell particles interacting with each other according to a screened Coulomb potential within the NAR-MMSA (nonadditive radius mean sphere approximation) model.[42] The micellar solution is considered as composed of uniformly sized ellipsoidal micelles with an aggregation number, N, and an effective charge Z. Within these assumptions the scattered intensity as a function of q can be written a

$$I(q) = (c - \mathrm{cmc})N\left(\sum_i b_1 - V_m\rho_s\right)^2 P(q)\, S(q) + I_{bkg} \quad (1)$$

where $(c - \mathrm{cmc})$ is the concentration of monomers aggregated in micelles composed of N monomers, b_i are the scattering lengths of each atom of the surfactant, V_m is the monomer volume, ρ_s is the scattering density of solvent, $P(q)$ is the orientation averaged intraparticle structure factor for ellipsoidal particles, $S(q)$ is the orientation averaged center−center interparticle structure factor, and the additive term takes into account incoherent scattering and electronic background signal. $P(q)$ and $S(q)$ are given, respectively, by[45]

$$P(q) = \int_0^1 |F(q,\mu)|^2 \, d\mu \quad (2)$$

$$S(q) = 1 + \frac{\langle |F(q,\mu)| \rangle}{\langle |F(q,\mu)|^2 \rangle}^2 [S_{MM}(q) - 1] \quad (3)$$

where $|F(q,\mu)|^2$ is the intraparticle structure factor for ellipsoidal two-shell micelles and μ is the direction cosine between the direction of the symmetry axis of the spheroid and the Q vector:

$$F(q,\mu) = f\frac{3j_1(u)}{u} + (1 - f)\frac{3j_1(n)}{n} \quad (4)$$

with

$$u = q[\mu^2 a^2 + (1 - \mu^2)b^2]^{1/2}$$

$$n = q[\mu^2 (a + d)^2 + (1 - \mu^2)(b + d)^2]^{1/2}$$

$$f = V_f(\rho_1 - \rho_2)/[\sum_i (b_i - V_m\rho_s)]$$

where b is the short axis of the ellipsoid, and the long principal axis, a, is determined by equating the volume of the inner core NV_m to the volume of the ellipsoid $(4\pi/3)b^2a$. $S_{MM}(q)$ has been calculated by solving the Ornstein−Zernicke equation for the pair correlation function within the NAR-MMSA closure that yields analytical solutions.[46]

Each micelle has been modeled as formed by a hydrophobic core of ellipsoidal shape (with principal axes a, b, b) that contains the surfactant hydrocarbon tails, where the solvent cannot penetrate, and a hydrated hydrophilic shell formed by the polar heads, a fraction of counterions, and some solvent molecules.

The core/shell contrast profile (see Scheme 2b) used in this analysis is justified by the comparison of the experimental spatial resolution, given by $2\pi/q_{max} \approx 9$ Å, and the sizes of the hydrocarbon chain and of the polar shell.

The contrast term can be calculated from the known chemical composition and volume of the surfactant, considered as uniform with respect to scattering length. Alternatively, if the spatial resolution is sufficient, we can conveniently divide the molecule in two different subregions of scattering lengths, that is, the hydrophobic chain and the polar-head region.

If the volume fraction of the scattering objects is known and the data are reduced in absolute units, the contrast term can be experimentally determined from the Porod invariant[47] without any assumption on size, shape, or correlation of the particles.

For a two-contrast system, in the presence of a sharp interface between the two scattering regions, the Porod invariant q is given by

$$q^* = \int_0^\infty I(q)\, q^2 \, dq = 2\pi^2(\Delta\rho)^2\phi_1(1 - \phi_1) \quad (5)$$

where ϕ_1 is the volume fraction of the aggregates and $\Delta\rho$ is the contrast term.

For triple contrast media, the extension of the Porod invariant leads to

$$q_{III} = 2\pi^2 \sum_i \phi_i \left(\sum_{j \neq i} \phi_j \Delta\rho_{ij}\right)^2 \quad (6)$$

where ϕ_i represents the volume fraction of the moiety i and $\Delta\rho_{ij}$ the contrast between phases i and j.

Once the contributions of the scattering from solvent and incoherent background are subtracted from the experimental spectra, the Porod invariant has been determined as follows:

$$q^* = \frac{I(q_{min})}{2} * {q_{min}}^3 + \int_{q_{min}}^{q_{max}} I(q)\, q^2\, dq + \frac{\text{intercept}}{q_{max}} \quad (7)$$

where q_{min} and q_{max} are the lowest and the highest limit of the experimental scattering vectors' range and "intercept" is the intercept of the best linear fit of the Porod limit. According to eq 5, a plot of the Porod's invariant as a function of $\phi_1(1 - \phi_1)$ yields a line whose slope is $2\pi^2\Delta\rho$.[2]

The experimental values of the Porod invariant (data not shown) for different surfactant volume fractions compared with those calculated assuming a simple two-contrast system (Scheme 2a) and a core−shell model (Scheme 2b) show a good agreement with the core−shell model that has been subsequently used for data analysis.

Equilibrium Surface Tension. Equilibrium surface tension was monitored with a KSV Sigma 70 digital tensiometer (accuracy 0.1mN/m) (Helsinki, Finland). Measurements were performed at 25 ± 0.5 °C, diluting a concentrated solution contained in a thermostated Teflon vessel. The solution was stirred for 1−5 min and allowed to equilibrate 10 min before data acquisition. Since the critical micellar concentration of DLPN occurs below 10^{-5} M, we have investigated the onset of micelle formation only for the diC$_8$PN derivatives.

UV and CD Adsorption. UV and circular dichroism (CD) spectra were recorded at room temperature (25 °C) with a Jasco J-715 (Tokyo, Japan) spectrophotometer using Hellma quartz cells, whose path length was in the 0.01−1 cm range, depending on the chromophore and concentration.

SCHEME 2: Homogeneous (a) and Core−shell (b) Models for the Scattering Length Density Profile of diC$_8$PU Arranged in Globular Micelles

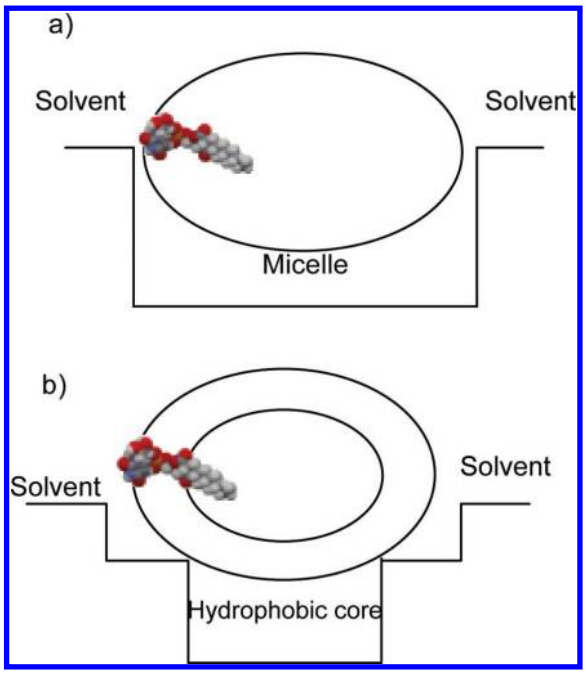

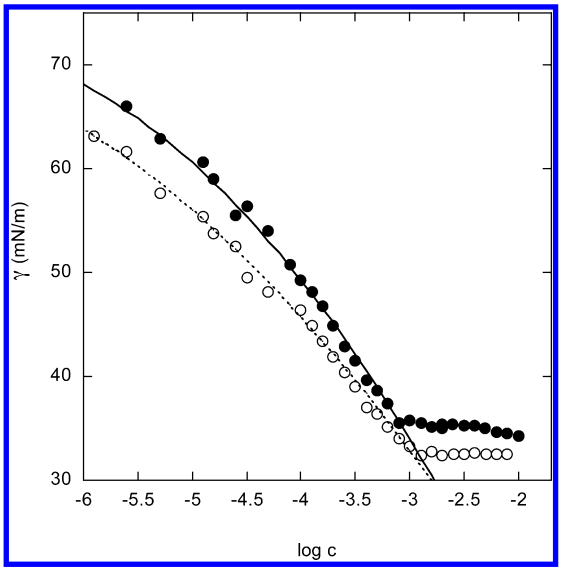

Figure 1. Surface tension curves for diC$_8$PA (●) and diC$_8$PU (○) in water.

TABLE 2: Surface Properties of diC$_8$PN in Water Compared with Those of the Homologous Phosphocholine (* Data Taken from Reference 45.)

	T (°C)	cmc × 10^4 (mol/L)	γ_{cmc} (mN/m)	A_{min} (Å^2/molecule)
diC$_8$PC*	40	1.6 ± 0.1	25.1	65 ± 4
diC$_8$PA	25	8.1 ± 0.2	35.7 ± 0.1	112 ± 4
diC$_8$PU	25	11.0 ± 0.2	32.5 ± 0.1	134 ± 3

Cryo-TEM. The preparation of the samples for Cryo-TEM investigation has been performed[48] as follow: a small droplet of the solution was placed under controlled conditions on a pretreated Cu grid of about 20 μm thickness, which was covered by a perforated cellulose acetate butyrate film. Excess material was removed by a gentle wiping off with a filter paper. The specimen was vitrified by a rapid transfer into liquid ethane close to its freezing temperature. The sample examination was performed with a Zeiss 902A electron microscope operating at 80 kV and 100 K. The temperature of the specimen was kept below −165 °C during both the transfer to the microscope and the examination. Images were recorded at underfocus settings of about 2−3 μm to enhance the image contrast.

Results and Discussion

Aggregation. The surface tension curves for diC$_8$PU and diC$_8$PA, Figure 1, are typical of micelle-forming surfactants. The break in the semilogarithmic plot marks the onset of aggregation into micellar structures. The steeper slope of surface tension curve for diC$_8$PA indicates that a larger surface excess at air/water interface occurs with a consequent compaction of the adsorption monomolecular film.

The critical micelle concentration, cmc, the surface tension at cmc, γ_{cmc}, related to the effective area per molecule at the saturated flat air/water interface, A_{min}, are reported in Table 2 for diC$_8$PA and diC$_8$PU together with the corresponding values found for corresponding phospholipids, diC$_8$PC, by Eastoe et al.[49] The exchange of choline with a nucleotide decreases the surface activity of the amphiphilic molecule: the surface tension at cmc is in fact in the range 32−36 mN/m at 25 °C for diC$_8$-PN compared to 25.1 mN/m at 40 °C for diC$_8$PC. This effect, larger in magnitude than the general effect of temperature on surface tension, is expected and ascribable to the presence of a net charge due to the nucleotide.

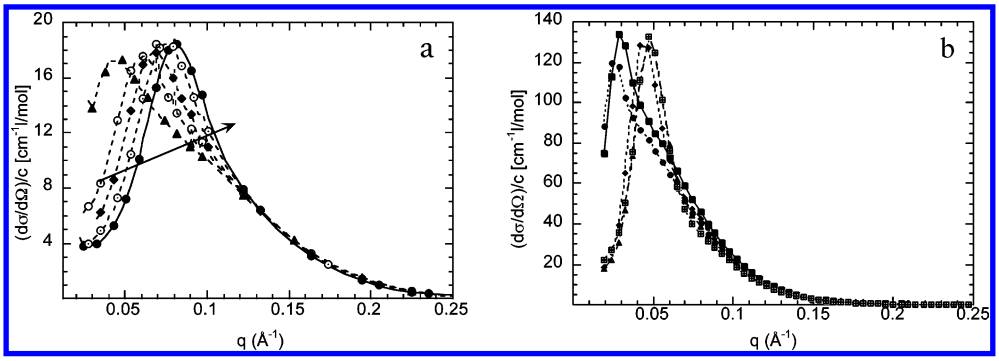

Figure 2. Small angle neutron scattering spectra of diC$_8$PU (a) and DLPU (b) in D_2O as a function of lipid concentration that increases in the direction indicated by the arrow.

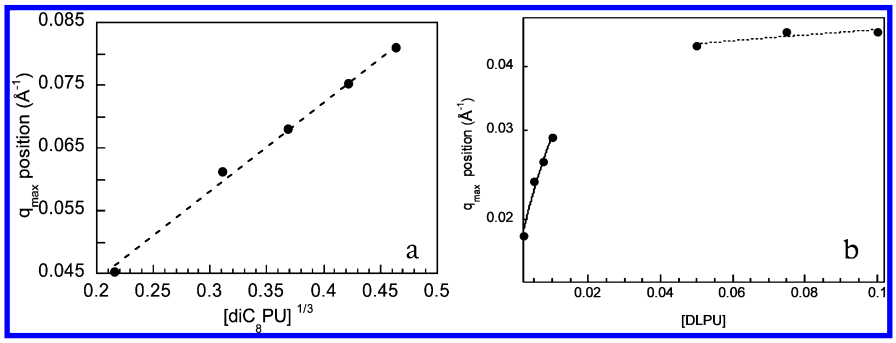

Figure 3. (a) Linear dependence of the position of the correlation peak (Å^{-1}); (b) Plot of q_{max} position vs lipid concentration for DLPU. The lines represent $c^{1/3}$ behavior in the low-concentration branch and $c^{1/2}$ in the higher concentration region.

Comparing the two derivatives, we notice that diC$_8$PU has both cmc and effective area per polar head higher than those of diC$_8$PA. Density measurements on isolated nucleosides (adenosine and uridine) in water yielded a partial molar volume of 170.8 ± 0.7 cm^3/mol (284 ± 1Å^3/molecule) for adenosine and 151.7 ± 0.5 cm^3/mol (251.9 ± 0.8 Å^3/molecule) for uridine.[50] Therefore the steric hindrance is higher for an isolated diC$_8$PA molecule.

Purines have higher stacking constants than pyrimidines (like uridine).[7] On a macromolecular scale this effect causes the fact that polyribouridylic acid (polyU) is a randomly coiled chain, with no conformational dependent hypochromicity and no anomalous optical rotatory dispersion. For polyriboadenylic acid (polyA), stacking interactions between adjacent bases occur instead and give rise to a secondary structure.

While the cmc scale (diC$_8$PA<diC$_8$PU) is expected on the basis of solubility considerations, the lower cross sectional area found for the bulkier derivative can be explained invoking stacking interactions between neighboring nucleic bases that induce a tighter arrangement of the polar-head groups at the interface. The presence of adenosine causes a more compact monolayer at air/water interface through interactions other than electrostatic and excluded volume, operating upon self-assembly but also responsible for a modulation of the self-assembly.

Following this first evidence, we have performed a structural characterization of the aggregates, in terms of size and shape to asses the effect of the hydrophobic contribution and of the base recognition properties on the self-assembly pattern.

Microstructural Characterization of the Aggregates: Effect of the Hydrophobic Portion. We have chosen to compare diC$_8$PU to DLPU. The former derivative has a packing parameter, often predictive of the self-assembled structure, around $^1/_3$ (see Scheme 1), while DLPU has a packing ratio slightly lower than $^1/_2$; for ionic surfactants this latter packing preference can be easily switched by adjustment of the ionic strength. In other words DLPU micellar solutions are responsive to ionic strength variations and can possibly exhibit extensive micellar growth.

Figure 2 shows the small angle neutron scattering spectra of diC$_8$PU and DLPU in D_2O as a function of nucleolipid volume fraction, normalized for the micellized surfactant concentration. The scattering patterns present a pronounced correlation peak, typical of ionic assemblies, indicating the occurrence of repulsive interactions between aggregates in the concentration range investigated. The peak position is dependent on lipid concentration and can be correlated to a mean interparticle distance. When a globular micellar structure is preserved in solution, the mean intermicellar distance, assuming a face-centered-cubic-like local ordering around a micelle, is given, according to Chen,[51] by

$$d = \frac{6.8559}{q_{max} - 0.0094} = \frac{1}{\sqrt{2}}\left\{\frac{4000N}{N_A[c]}\right\}^{1/3} \times 10^8\ \text{Å} \qquad (8)$$

where q_{max} is the abscissa of the correlation peak, c is the molar concentration, and N is the aggregation number. The shift of the correlation peak can be explained by a decrease of the positional correlation length, caused by an increase of micellar volume fraction.

The good linear correlation between q_{max} and $c^{1/3}$, for the spectra of diC$_8$PU, shown in Figure 3a provides a first hint of the substantial invariance of the globular shape of the aggregates, as concentration is increased. The aggregation numbers for quasi-spherical micellar aggregates derived with this simple model are reported in the second column of Table 3.

Even in the case of diC$_8$PU, the presence of the correlation peak hampers a straightforward quantitative analysis of the form factor, necessary to assess whether the shape of the aggregates is concentration invariant. A Porod representation (i.e., a plot of $I(q)xq^4$ vs q, not shown), highlights the coincidence of the maxima and the minima for the oscillations of the form factor. Assuming a spherical shape, one can infer a micellar radius of

TABLE 3: Main Parameters Extracted through Model Fitting of the Spectra Reported in Figure 2

sample	N^*[a]	N[b]	a/b[c]	b (Å)	α[d]	δ(Å)[e]
A	39	38	1.65	13.0	0.35	9.0
B	36	36	1.56	13.0	0.36	9.0
C	34	33	1.51	12.9	0.33	9.1
D	30	31	1.36	13.0	0.32	9.0
E	27	28	1.21	13.0	0.30	9.0

[a] N^* = aggregation number from eq 8. [b] Aggregation number. [c] Axial ratio for the ellipsoidal micelle with axes *a*, *b*, *b*. [d] Fractional charge, given by *Z*/N. [e] Thickness of the hydrophilic shell.

24 Å from the positions of the maxima and the minima ($qR = \pi(^3/_2)^{1/2}$ for the first maximum). This model-free analysis supports the presence of globular aggregates and their shape invariance in this concentration range. We have performed more sophisticated analysis assuming the presence of ellipsoidally shaped micelles formed by a hydrophobic core and hydrophilic shell interacting through a screened Coulomb potential.

According to this model, variations of the experimental spectra of diC_8PU can be interpreted as mainly due to an increase in correlation, while the growth of micellar aggregates and their shape change is less important. The fitting parameters extracted from SANS spectra of diC_8PU micelles are reported in Table 3. Columns two and three report the aggregation numbers evaluated from eq 8 and extracted from the fitting results, respectively: the agreement is excellent and confirms that the simple model-free analysis was essentially correct. While the apolar core radius and the hydrophilic thickness are practically invariant and consistent with the surfactant structure, the asymmetry of the aggregates monotonously rises as lipid concentration is increased and micellar charge density is decreased.

A first inspection of DLPU SANS spectra (Figure 2b) shows, similarly to diC_8PU, the presence of a peak in the low-*q* range, indicating the presence of interparticle correlation due to repulsive interactions between charged micelles. However, the scaling of the peak position, reported in Figure 3b, is more complicated indicating the apparent presence of two different regimes: for the lowest volume fractions, a substantial globularity is obeyed, while for higher volume fractions, a linear dependence of q_{max} from $c^{1/2}$ can be attributed to the presence of cylindrically elongated structures. This series of spectra show differences not only in the position of the correlation peak, as for diC_8PU, but also in the intermediate *q*-range, indicating variation of local structure of the aggregates. If we compare the spectrum obtained for a given volume fraction of micellized surfactant for diC_8PU and DLPU, (Figure 4) the effect of a substantial increase of the chain length of the surfactant becomes evident. The spectrum of DLPU is consistent with the presence of larger aggregates and the position of the intraparticle correlation peak (occurring at a lower value of the scattering vector) indicates a lower scaling exponent with volume fraction. Therefore we expect the presence of elongated aggregates grown along the axial direction.

Aqueous solutions of ionic surfactants can exhibit a considerable micellar growth to elongated flexible cylindrical micelles as a response to a variation of control parameters (typically, surfactant volume fraction and ionic strength) to form very large anisotropic aggregates.[26−28] A qualitative explanation of this phenomenon can be found in the salt dependence of the surfactant "packing parameter".[52] For $c >$ cmc, a further increase in concentration generally causes micelles to grow because of mass-action effects. For typical ionic surfactants that prefer spherical packing, this growth is generally very limited;

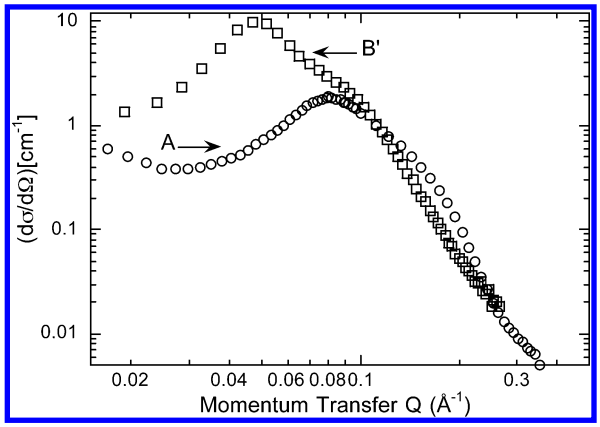

Figure 4. Comparison of the spectra corresponding to the same volume fraction of micellized lipid (5.0%) for sample A (diC_8PU 1.0×10^{-1} mol/L) and sample B′ (DLPU 7.5×10^{-2} mol/L).

TABLE 4: Structural Parameters of DLPU Micelles as a Function of Lipid Concentration in D_2O

[lipid]	N[a]	a/b[b]	b (Å)	α[c]	δ (Å)[d]
1.0×10^{-1}	178.0	3.5	18.1	0.14	10.3
7.5×10^{-2}	143.5	2.7	18.3	0.19	10.6
5.0×10^{-2}	123.1	2.2	18.7	0.20	10.2
1.0×10^{-2}	105.4	1.9	18.6	0.19	10.0
7.5×10^{-2}	103.0	1.9	18.5	0.18	10.2
5.0×10^{-2}	100.0	1.7	19.0	0.17	10.2
2.0×10^{-3}	90.6	1.7	18.3	0.19	10.2
1.0×10^{-3}	73.3	1.4	18.4	0.20	10.3

[a] Aggregation number. [b] Axial ratio for the ellipsoidal micelle with axes a, b, b. [c] Fractional charge, given by *Z*/*N*. [d] Thickness of the hydrophilic shell.

however, at high ionic strength, intramicellar repulsive interactions are screened, favoring a locally cylindrical packing that provides a possibility for an uniaxial growth. When interparticle distance becomes of the same order of magnitude of the aggregate size, micelles start to entangle and flow properties of the surfactant solution become reminiscent of polymers in semidilute conditions, showing viscoelastic behavior.[53,54]

The contour length is determined by concentration and by the extent of free energy minimization that a surfactant molecule gains if packing along the cylindrical body of the aggregate instead of the hemispherical end-caps, ΔE. This quantity depends on the variation of the above-mentioned control parameters (surfactant volume fraction, ionic strength,). When this term is favorable, micelles can become very long aggregates characterized by a certain degree of flexibility, depending on their surface charge density and on the chemical nature of the surfactant.

For a more quantitative analysis of DLPU spectra we have adopted the same model illustrated for diC_8PU; the quantity of interest here is the axial ratio, which indicates the degree of asymmetry of the aggregate and is 1 for a perfectly spherical aggregate. Conventionally the aggregates are assumed as globular when this ratio is below 2 (Table 4).[55] In this case the intraparticle and interparticle structure factors (data not shown), extracted with the best fitting procedure, show a consistent dependence on lipid volume fraction.

A parallel concentration scan in 0.1 M phosphate buffered solution at pH 7.5[56−59] (I = ionic strength = 0.25 mol/L) is in agreement with flexible elongated objects that, already at volume fractions as low as 0.06%, while at ∼1.2% ([DLPU] = 2.0×10^{-2} mol/L) start to entangle to form a micellar transient network. In the present case the absence of salt, while causing interaggregate electrostatic repulsion, should favor a higher

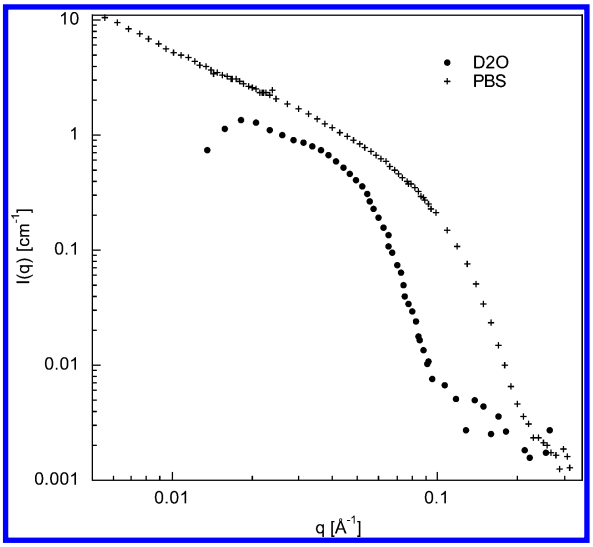

Figure 5. SANS spectra of DLPU 1×10^{-2} M ($f = 0.6\%$) in D_2O and in phosphate buffered solution highlighting micellar growth for the system at higher ionic strength.

micellar rigidity. A relatively modest increase of ionic strength is sufficient to switch the growth to extremely elongated objects, as shown for the 1.0×10^{-2} mol/L sample in D_2O and 0.1 M PBS, respectively (Figure 5).

A similar effect is not found for diC_8PN derivatives; we have already reported a SANS characterization of the aggregates in the same buffer for two different concentrations (1.0×10^{-2} mol/L and 3.5×10^{-2} mol/L). A slight increase in aggregation number and aggregate asymmetry does not cause deviations from globularity.[42] This can be appreciated comparing the cryo-TEM pictures, Figure 6, obtained for 3.5×10^{-2} mol/L diC_8-PU in PBS and 1.0×10^{-2} mol/L DLPU in the same medium. Globular uniform micelles of diC_8PU can be recognized notwithstanding the relatively high volume fraction while the occurrence of long and flexible aggregates is easily recognizable for DLPU. Cryo-TEM substantially confirms the results obtained from scattering, leading to the overall conclusion that, while a globular shape is retained for diC_8PU derivatives, packing preferences of DLPU are easily switched so that locally cylindrical aggregates are formed, whose contour length can be tuned by variation in ionic strength.

DLPN derivatives represent therefore a responsive assembler, where shape and dimensionality of the aggregates are externally and reversibly tuned by ionic strength modulations.

Microstructural Characterization of the Aggregates: Effect of the Polar Head. Micellization thresholds and surface areas obtained for the short-chain derivatives have been discussed in terms of different stacking properties of the bases, rather than charge and excluded volume; this will be further developed in terms of structural properties of the aggregates in the next paragraphs.

As anticipated, this effect is a microstructural fine-tuning, which is more appreciable from scattering when intraparticle correlation is screened; therefore the following discussion concerns aggregation in PBS medium.

For short chain derivatives the higher aggregation number found for diC_8PA with respect to diC_8PU is accompanied in PBS by a lower cross sectional area per phospholipid chain; also the number of water molecules occupying the interfacial corona is lower.[42,60] We have attributed this effect to the displacement of solvent caused by a stacked configuration of the bases, which is supported by the experimental evidence of a lower surface area at the a/w interface below the aggregation

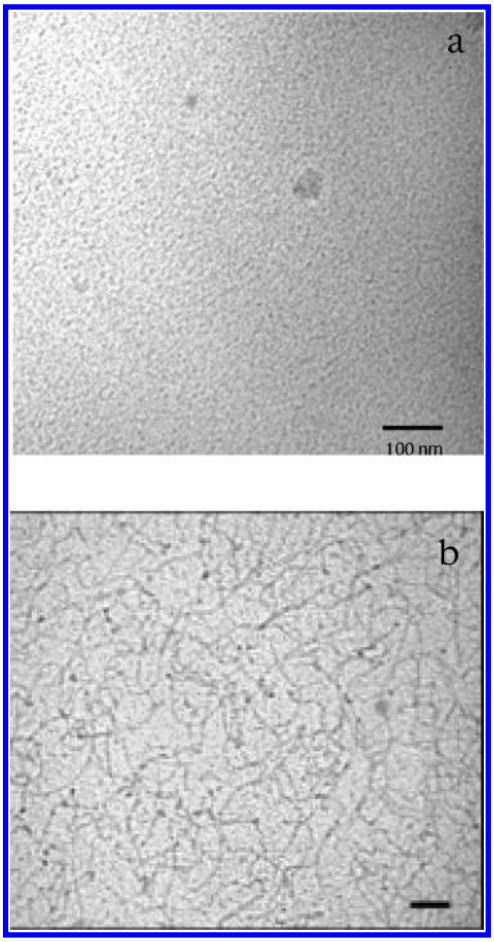

Figure 6. Cryo-TEM pictures of micellar aggregates formed by (a) diC_8Pu (3.5×10^{-2} M) and (b) DLPU (1×10^{-2} M). The bar is 100 nm.

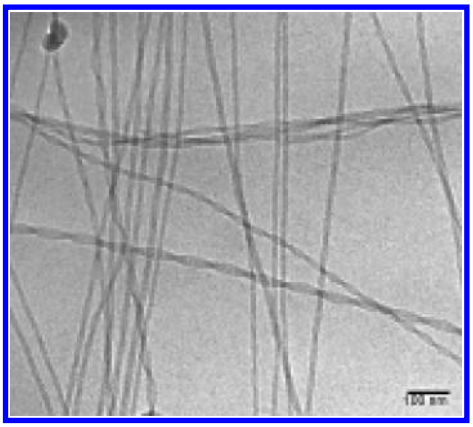

Figure 7. Cryo-TEM pictures of micellar aggregates formed DLPA (1×10^{-2} M). The bar is 100 nm.

threshold. We have to take into account that molecular packing preferences for these derivatives are skewed toward high positive curvatures, as sketched in Scheme 1. The high interfacial curvature should disfavor base interactions with respect to lower interfacial curvature, found for instance in cylindrical micelles.

The effect of base substitution should be therefore more apparent for DLPN derivatives. Figure 7 shows a cryo-TEM picture for 1.0×10^{-2} DLPA in PBS, obtained 3 days after preparation; the different morphology of the aggregates with respect to DLPU can be appreciated by comparing this picture with Figure 6b.

Freshly prepared DLPA solutions are mostly composed of threadlike micelles whose cross-section size is about 5 nm. The

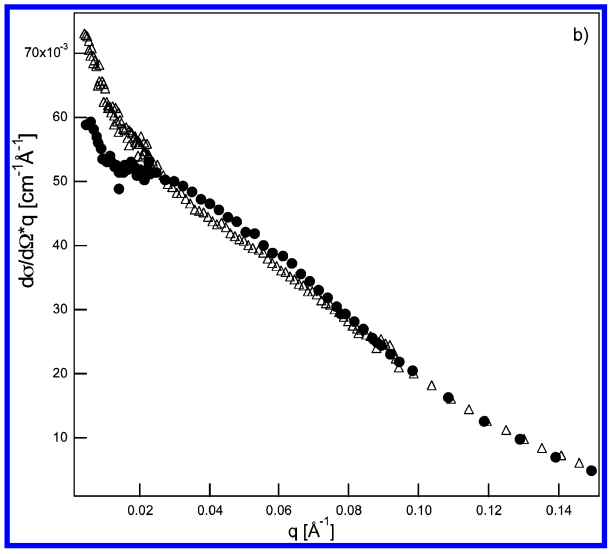

Figure 8. Holtzer plot of DLPA (△) and DLPU (●) samples 1×10^{-2} M in PBS 0.1 M at pH = 7.5.

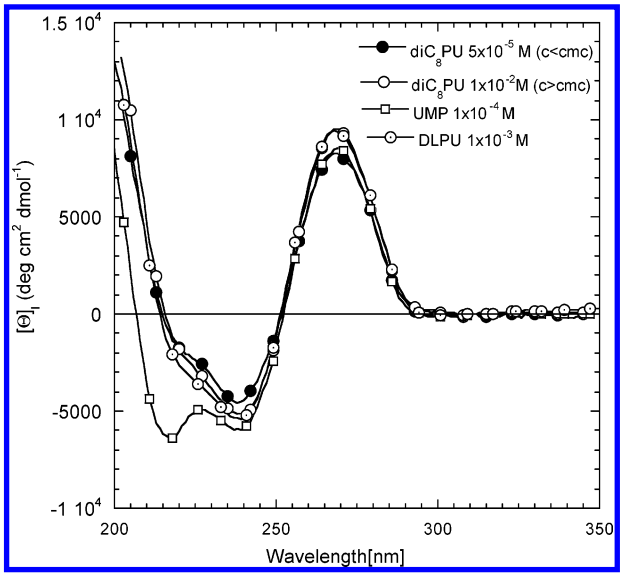

Figure 9. CD spectra of UMP, diC_8PU (below and above cmc), and DLPU solutions in PBS.

observed time evolution of the aggregate morphology, accompanied by the appearance of an ultraslow relaxation in quasi-elastic light scattering,[58] arises from a hierarchical aggregation of wormlike structures identical to DLPU micelles.[59] This is due to stacking and H-bonding between the nucleic bases (made possible by the hydrophobic interactions of the alkyl-chain moieties), as also observed by Yanagawa et al.[61] by aging both di-C_{16}P-cytidine and di-C_{14}P-cytidine vesiscles at 25 C for 1 day.

None of these effects can be noticed for DLPU solutions (weaker homostacker), composed of wormlike micelles that have been investigated in wide concentration and salinity ranges through a combination of SANS and static and quasi-elastic light scattering.[56−58] The data for DLPU have been interpreted through a nonlinear least-squares fitting of the experimental spectra by parametrized wormlike chain scattering functions, obtained with Monte Carlo methods, which allow an accurate estimate of micellar flexibility in terms of persistence length (230 Å). The picture that emerges is a continuous increase in contour length and invariance of a cylindrical local structure, with cross sectional radius of 20 Å.

The SANS spectra of two representative samples (DLPA and DLPU 1.0×10^{-2} M) are reported in Figure 8 as bending-rod or Holtzer plots, (I(q)xq vs q). The q^{-1} scattering law, that is, the fingerprint of a cylindrical structure, is observed for DLPU micelles as a flat portion in the low-q region, marking the momentum transfer range where neutrons probe a locally rigid rod; the upturn switch is instead an indication of the global flexibility of the aggregates. For DLPA, the absence of such a portion in the small-q region and the fact that spectra do not coincide in the intermediate q range, account for a different local structure. Also, a Porod representation of the same spectra (not shown here) rules out the presence of identical local structures.

A precise analysis of DLPA spectra is complicated by the fact that possibly several structures are simultaneously present. Without going further into details, it is important to stress here how subtly different polar-head properties, acting on a local scale, propagate in the mesoscopic domain, causing dramatic variations in the aggregation pattern.

What Drives Microstructure? A Spectroscopic Study. Spectroscopic investigation through circular dichroism of diC_8PN and DLPN aggregates allows investigating specific interactions which are different in the two cases: for diC_8PN it is possible to monitor conformational changes brought about by aggregation, while for DLPN (responsive aggregates) we can observe the variation induced by modulation of interfacial curvature.

CD spectra reflect mainly the properties of the headgroup area, as the choromophores (nucleobases) are localized in the region of the headgroup of the phospholipids.

From the classical literature on nucleic acids, it is known that $\pi \rightarrow \pi^*$ transitions, polarized in the plane of the base, are mainly responsible for UV adsorption bands,[62] together with $n \rightarrow \pi^*$ transitions due to nonbonding N and O electron pairs, polarized perpendicularly with respect to the base plane. For purine and pyrimidine chromophores, the characteristic absorption band in the 250−280 nm region contains the B_{2u}, B_{1u}, and one or more $n \rightarrow \pi^*$ transitions. The two bands derived from the doubly degenerate A_{1g} and E_{1u} (E_{1ua} and E_{1ub}) benzene transitions are usually found in the 180−220 nm region. For uridine derivatives the common CD pattern is given by the typical positive, negative, negative, positive trend. These four Cotton effects are found in the UV range 190−300 nm and are correlated each to one of the four electronic transitions above. For the adenine nucleoside derivatives a single negative CD band, ascribed to B_{2u} transition around 260 nm, is reported together with two Cotton effects, negative around 220 nm and positive around 200 nm.

Figure 9 shows the CD spectra of diC_8PU, below and above the cmc in water at pH 7, together with DLPU at 1.0×10^{-2} M. The chromophore signal is not dependent on its concentration and on the aggregation state, compared to that obtained for UMP. The only difference concerns the E_{1ua} band and is due to the 5′ insertion of lipid tail. The unchanged positive sign of the CD band correlated with B_{2u} is indicative that the torsion angle is in the range of anti conformations, which therefore is unaltered by the presence of lipidic tail or by self-assembly.

A completely different behavior is found for diC_8PA, Figure 10. DiC_8PA shows for $c \ll$ cmc a positive CD band centered at 260 nm, then a negative signal at 215 nm and a positive one of the same magnitude at 204 nm. Around 260 nm, AMP shows main absorptions of opposite sign. The presence in the nucleolipid molecule of double hydrocarbon chain induces an apparent conformational variation in the polar-head group portion with respect to AMP. The effect observed for diC_8PA is the same

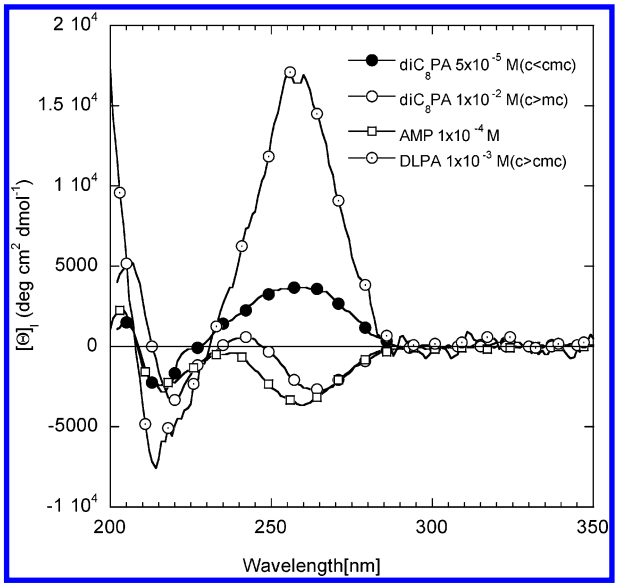

Figure 10. CD spectra of AMP, diC_8PA (below and above cmc), and DLPA solutions.

observed and theoretically predicted[34] for adenosine derivatives in anti conformation. Micellization causes a further conformational rearrangement, which is then retained for the concentration range here explored.

DLPA measured above the aggregation threshold has similarly complicated concentration dependence. At low volume fractions the behavior is qualitatively similar to diC_8PA below the aggregation threshold, even if molar ellipticities are noteworthy higher. Increasing surfactant volume fractions (spectra not shown) causes a sign reversal of this Cotton effect, with a behavior similar to the micellized diC_8PA. These results confirm that that microstructure and base conformation are interplaying for DLPA.

Molecular Recognition According to a Watson−Crick Pattern: Microstructure and Spectroscopic Properties. To monitor molecular recognition between nucleolipids in micelles, we have to show that additional cooperative effects are acting when two derivatives bearing Watson−Crick complementary polar heads are mixed and that the observed property show deviations from the ideal behavior driven by the entropy of mixing. It is worthwhile to stress that the nucleolipids have identical apolar parts and are negatively charged: if no specific interactions are present mixing should be ideal.

We have previously reported evidence for a minimum deviation of the cmc of the mixed system 1:1 = diC_8PU/diC_8PA according to a Holland−Rubingh approach,[41] and for an area contraction per amphiphile molecule on micelles when both derivatives are present.[42] This effect is accompanied by spectroscopic evidence of base stacking at the interface and of H-bonding between the two derivatives obtained through NMR spectroscopy in micelles. Circular dichroism was also employed to prove additional base interactions in the mixed system.

We report here the important evidence that the nonideality is distinctive for micelles. Figures 11 and 12 report CD spectra for diC_8PA, diC_8PU and the 1:1 mixed systems compared to the "ideal" spectrum computed from binary systems. Below the cmc the mixture is indistinguishable from the "ideal" spectrum, while above the cmc there is an excess CD effect (which is then invariant for higher concentrations). It is not straightforward to ascribe the observed effect to a precise interaction pattern, however this piece of evidence is a clear-cut demonstration of the role played by aggregation, which is somehow similar to macromolecular organization for polynucleotides.

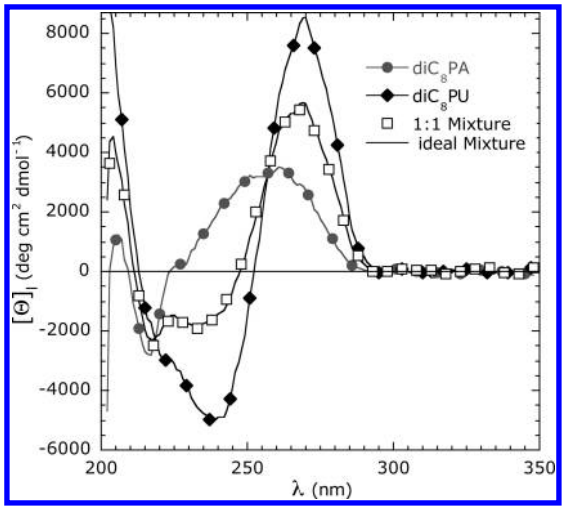

Figure 11. CD spectra of diC_8PA, diC_8PU, diC_8PA/diC_8PU (1:1) below cmc; the continuous line (coinciding with the experimental spectrum obtained from diC_8PA/diC_8PU) is the spectrum computed from binary solutions.

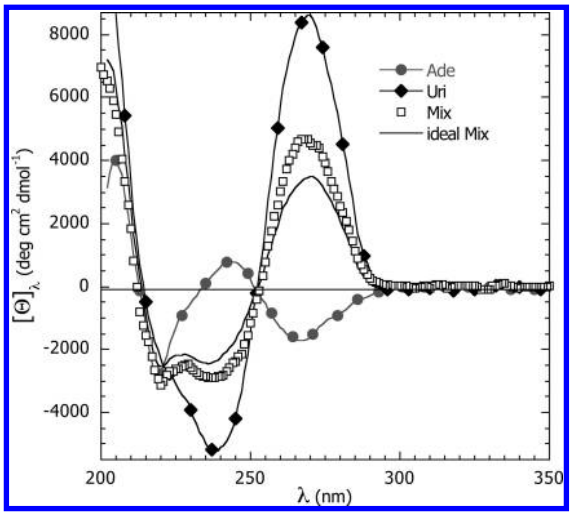

Figure 12. CD spectra of diC_8PA, diC_8PU, diC_8PA/diC_8PU (1:1) above cmc; the continuous line (*not* coinciding with the experimental spectrum obtained from diC_8PA/diC_8PU) is the spectrum computed from binary solutions.

Therefore, there is a interplay between aggregation and molecular recognition: in other words, nonideality is absent for monomeric solution and distinctive for self-assemblies.

The same analysis for DLPN is hampered by the extremely low critical concentration aggregations. CD studies of DLPM micellar solutions (obtained by mixing of two equimolar solutions of DLPA and DLPU) above cmc have been previously presented[59] by us, and the deviation either from the ideal mixing or from the segregation of the lipids was clearly inferred, indicating the presence of specific interactions between nucleic bases at the interface. As seen in the previous paragraph for DLPA, the presence of specific interactions between polar heads has a major impact on aggregation.

The similarity of the 1:1 mixture to the behavior displayed by DLPA, which then dictates self-aggregation, can be further appreciated through the observation of a representative cryo-TEM picture shown in Figure 14, where helicoidally wrapping micelles are clearly visible.

Figure 13 reports the SANS spectra of 1×10^{-3} mol/L DLPN series in PBS. In particular DLPA and DLPM group together and differ from DLPU behavior that is typical of a pure wormlike phase. In the low-q region the scaling law is similar,

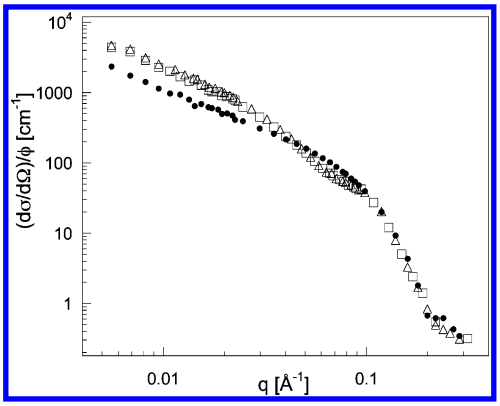

Figure 13. SANS spectra of 1×10^{-3} M DLPA (△), DLPU (●), and DLPA/DLPU (1:1) (□) micellar solutions in PBS 0.1 M at pH = 7.5.

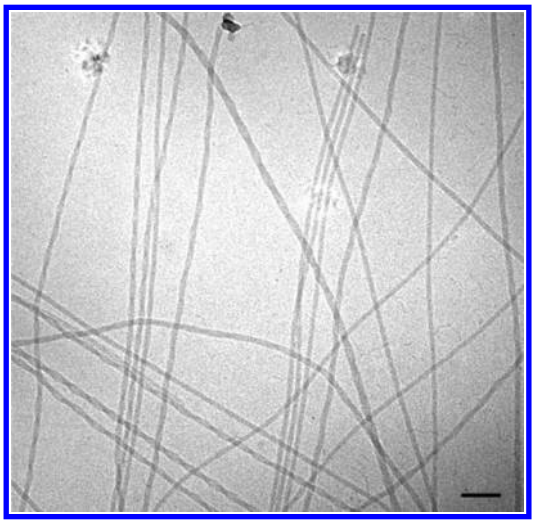

Figure 14. Cryo-Tem pictures of micellar aggregates formed by DLPA/DLPU (1:1) in PBS 0.1 M at pH = 7.5 (total lipid concentration is 1×10^{-3} M). The bar is 100 nm.

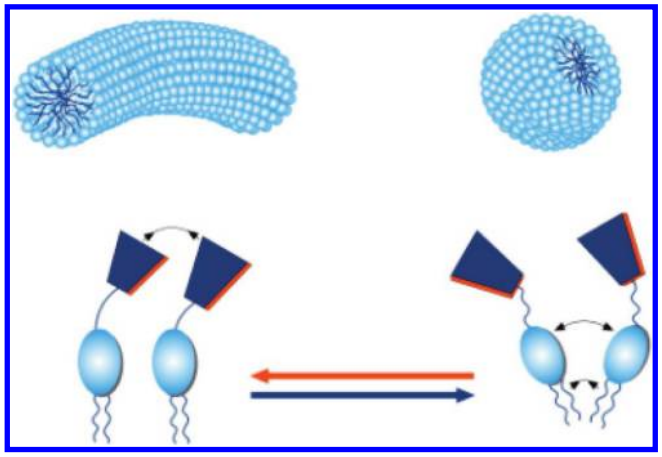

Figure 15. A cartoon depicting the possible mechanism of different effects of base−base interactions on microstructures: the self-assembly dimensionality is mainly ruled by the hydrophobic portion and is globular for short chain diC_8PN and cylindrical for DLPN. The lower interfacial curvature allows closer and better oriented base−base interactions, which are then responsible for a more efficient modulation on microstructure itself.

even if the forward scattering is considerably higher for DLPA and DLPM, but a definitely different behavior is exhibited in the intermediate-*q* region, where these latter derivatives show a switch to a negative scaling exponent between 1.5 and 2. The formation of helical structures, as said above, arises from hierarchical aggregation of wormlike structures identical to DLPU micelles,[59] and thus, the complete determination of the structural features in the direct space is greatly complicated not only by the concentration variance of such parameters like polydispersity and interactions but also by the likely simultaneous presence of different structures.

Conclusions

Aggregates formed by phosphatidylnucleosides merge the responsiveness of conventional ionic self-assemblies to the additional tunability ruled by molecular recognition between complementary bases owing to their DNA-like polar head. These factors interplay in determining the phase behavior and aggregate microstructure: a complete picture of these effects can be inferred by comparison of diC_8PN and DLPN.

For diC_8PN molecular recognition plays a definite role in the thermodynamics of aggregation, as demonstrated for short-chain derivatives. Additional synergic effects can be observed in the aggregation of a 1:1 mixture of nucleolipids bearing complementary base substitution. After aggregation, though spectroscopic properties typical of recognition can be observed, the effects of polar-head specificity on microstructure are minor for diC_8PN, possibly because of the higher curvatures imposed by the packing parameters. A slight increase of the packing ratio promotes a more responsive self-aggregation behavior to external factors and a stronger impact of the polar-head nature, that becomes determinant for DLPN, as sketched in Figure 15.

Acknowledgment. The authors wish to thank CSGI and MIUR (PRIN-2006) for funding the research. European Union financing is acknowledged for SANS experiments at the European Neutron Facilities LLB in Paris and HMI in Berlin (contract number RII3-CT-2003-505925 (NMI3)). F.B.B. acknowledges financial support from the European Commission's Sixth Framework Programme (Project reference AMNA, Contract No. 013575). Dr. Goran Karlsson and Prof. Mats Almgren are acknowledged for cryo-TEM experiments. We also would like to thank Mr. Paolo Parri for his help in preparing art works.

References and Notes

(1) Fuhrhop, J. H.; Koning, J. *Membrane and Molecular Assemblies: the Synkinetic Approach*; The Royal Society of Chemistry: London, 1994.
(2) Bonini, M.; Berti, D.; Di Meglio, J. M.; Almgren, M.; Teixeira, J.; Baglioni, P. *Soft Matter* **2005**, *6*, 444.
(3) Ambrosi, M.; Fratini, E.; Alfredsson, V.; Ninham, B. W.; Giorgi, R.; Lo Nostro, P.; Baglioni, P. *J. Am. Chem. Soc.* **2006**, *128*, 7209.
(4) Luk, Y. Y.; Abbott, N. L. *Curr. Opin. Colloid Interface Sci.* **2002**, *7*, 267.
(5) Rosemeyer, H. In *Chemistry & Biodiversity*; Verlag Helvetica Chimica Acta AG: Zurich, 2005; Vol. 2; pp 977.
(6) Tu, R. S.; Tirrell, M. *Adv. Drug Delivery Rev.* **2004**, *56*, 1537.
(7) Saenger, W. *Principles of Nucleic Acid Structure*; Springer-Verlag: New York, 1984; Vol. cap. 6; pp 116.
(8) Tielmann, P.; Marchal, A.; Lehn, J. M. *Tetrahedron Lett.* **2005**, *46*, 6349.
(9) Ghoussoub, A.; Lehn, J. M. *Chem. Commun.* **2005**, *46*.
(10) Seeman, N. C. *Angew. Chem., Int. Ed.* **1998**, *37*, 3220.
(11) Storhoff, J. J.; Mirkin, C. A. *Chem. Rev.* **1999**, *99*, 1849.
(12) Niemeyer, C. M. *Angew. Chem., Int. Ed.* **2001**, *40*, 4128.
(13) Storhoff, J. J.; Lazarides, A. A.; Letsinger, R.; Schatz, G. C. *J. Am. Chem. Soc.* **2000**, *122*, 4640.
(14) Ding, B.; Seeman, N. C. *Science* **2006**, *314*, 1583.
(15) Feldkamp, U.; Niemeyer, C. M. *Angew. Chem.* **2006**, *45*, 1856.
(16) Tumpane, J.; Sandin, P.; Kumar, R.; Powers, V. E. C.; Baglioni, P.; Lehn, J. M.; Albinsson, B.; Lincoln, P.; Wilhelmsson, L. M.; Gale, N.; Brown, T.; Nordèn, B. *Chem. Phys.* Letters **2007**, *440*, 125.
(17) Schwender, R. A.; Gowland, P.; Horber, D. H.; Zahner, R.; Schertler, A.; Schott, H. *Antiviral Res.* **1994**, *24*, 79.
(18) Heiati, H.; Tawashi, R.; Phillips, N. C. *Int. J. Pharm.* **1998**, *174*, 71.
(19) Moreau, L.; Barthélémy, P.; M. El Maataoui; Grinstaff, M. W. *J. Am. Chem. Soc.* **2004**, *126*, 7533.

(20) Arigon, J.; Prata, C. A. H.; Grinstaff, M. W.; Barthélémy, P. *Bioconjug. Chem.* **2005**, *16*, 864.
(21) Arigon, J.; Prata, C. A. H.; Grinstaff, M. W.; Barthelemy, P. *Bioconjug. Chem.* **2005**, *16*, 864.
(22) Iwaura, R.; Yoshida, K.; Masuda, M.; Yase, K.; Shimizu, T. *Chem. Mater.* **2002**, *14*, 3047.
(23) Iwaura, R.; Yoshida, K.; Masuda, M.; Ohnishi-Kameyama, M.; Yase, K.; Shimizu, T. *Angew. Chem., Int. Ed.* **2003**, *42*, 1009.
(24) Shuto, S.; Ueda, S.; Imamura, S.; Fukukawa, K.; Matsuda, A.; Ueda, T. *Tetrahedron Lett.* **1987**, *28*, 199.
(25) Berti, D.; Franchi, L.; Baglioni, P.; Luisi, P. L. *Langmuir* **1997**, *13*, 3438.
(26) Itojima, Y.; Ogawa, Y.; Katsushige, T.; Handa, N.; Ynagawa, H. *Biochemistry* **1992**, *31*, 4757.
(27) Yeagle, P. *The Structure of Biological Membranes*; CRC Press: Boca Raton, FL, 1992.
(28) Cevc, G.; Marsh, D. *Phospholipid Bilayers Physical Principles and Models*; Wiley & Sons: 1987; Vol. 5.
(29) Katsaras, J.; Gutberlet, T. *Lipid Bilayers: Structure and Interactions*; Springer, 2000.
(30) El-Sayed, M. Y.; Roberts, M. F. *Biochim. Biophys. Acta* **1985**, *831*, 133.
(31) El-Sayed, M. Y.; De Bose, C. D.; Coury, L. A.; Roberts, M. F. *Biochim. Biophys. Acta* **1985**, *837*, 325.
(32) Lewis, K. A.; Bian, J.; Sweeney, A.; Roberts, M. F. *Biochemistry* **1990**, *29*, 9962.
(33) Israelachvili, J. N.; Mitchell, D. J.; Ninham, B. W. *J. Chem. Soc., Faraday Trans.* **1976**, *72*, 1525.
(34) Lin, T.-L.; Chen, S.-H.; Gabriel, N. E.; Roberts, M. F. *J. Am. Chem. Soc.* **1986**, *108*, 3499.
(35) Lin, T.-L.; Chen, S.-H.; Gabriel, N. E.; Roberts, M. F. *J. Phys. Chem.* **1987**, *109*, 2321.
(36) Tausk, R. J. M.; Karmiggelt, J.; Oudshoorn, C.; Overbeek, J. T. *Biophys. Chem.* **1974**, *1*, 175.
(37) Tausk, R. J. M.; Van Esch, J.; Karmiggelt, J.; Voordouw, G.; Overbeek, J. T. *Biophys. Chem.* **1974**, *1*, 184.
(38) Tausk, R. J. M.; Oudshoorn, C.; Overbeek, J. T. *Biophys. Chem.* **1974**, *2*, 53.
(39) Tausk, R. J. M.; Overbeek, J. T. *Biophys. Chem.* **1974**, *2*, 175.
(40) Berti, D.; Bonaccio, S.; Barsacchi-Bo, G.; Luisi, P. L.; Baglioni, P. *J. Phys. Chem. B* **1998**, *102*, 303.
(41) Berti, D.; Barbaro, P. L.; Bucci, I.; Baglioni, P. *J. Phys. Chem B* **1999**, *103*, 4916.
(42) Berti, D.; Pini, F.; Teixeira, J.; Baglioni, P. *J. Phys. Chem. B* **1999**, *103*, 1738.
(43) Banchelli, M.; Berti, D.; Baglioni, P. *Angew. Chem.* **2007**, *46*, 3070.
(44) Keiderling, U. *BerSANS Data reduction Manual;* HMI: Berlin, 1994.
(45) Sheu, E. Y.; Chen, S.-H.; Huang, J. S. *J. Phys. Chem.* **1987**, *91*, 1535.
(46) Liu, Y. C.; Baglioni, P.; Teixeira, J.; Chen, S. H. *J. Phys. Chem.* **1994**, *98*, 10208.
(47) Cantú, L.; Corti, M.; Del Favero, E.; Dubois, M.; Zemb, T. N. *J. Phys. Chem. B* **1998**, *102*, 5737.
(48) Mays, H.; Almgren, M.; Dedinaite, A.; Claesson, P. M. *Langmuir* **1999**, *15*, 8072−8079.
(49) Eastoe, J.; Dalton, J. S.; Heenan, R. K. *Langmuir* **1998**, *14*, 5719.
(50) Patel, S. G.; Kishore, N. *J. Solution Chem.* **1995**, *24*, 25.
(51) Chen, S.-H.; Sheu, E. Y.; Kalus, J.; Hoffmann, H. *J. Appl. Crystallogr.* **1988**, *21*, 751.
(52) Magid, L. J. *Langmuir* **1998**, *102*, 4064.
(53) Cates, M. E.; Candau, S. J. *J. Phys. Condens. Matter* **1990**, *2*, 6869.
(54) Cates, E. M. *J. Phys.* (*Paris*) **1988**, *49*, 1593.
(55) Missel, P. J.; Mazer, N. A.; Benedek, C. Y.; Young, M. C.; Carey, J. *J. Phys. Chem.* **1980**, *84*, 1044.
(56) Baldelli Bombelli, F.; Berti, D.; Pini, F.; Keiderling, U.; Baglioni, P. *J. Phys. Chem. B* **2004**, *108*, 16427.
(57) Baldelli Bombelli, F.; Berti, D.; Keiderling, U.; Baglioni, P. *Appl. Phys. A* **2002**, *74* [Suppl.], S1270.
(58) Baldelli Bombelli, F.; Berti, D.; Keiderling, U.; Baglioni, P. *J. Phys. Chem. B* **2002**, *106*, 11613.
(59) Baldelli Bombelli, F.; Berti, D.; Almgren, M.; Karlsson, G.; Baglioni, P. *J. Phys. Chem. B* **2006**, *110*, 17627.
(60) Berti, D.; Pini, F.; Texeira, J.; Baglioni, P. *Physica B* **2000**, *276*, 334.
(61) Yanagawa, H.; Ogawa, Y.; Furuta, H.; Katsushige, T. *J. Am. Chem. Soc.* **1989**, *111*, 4567.
(62) Hug, W.; Tinoco, J. *J. Am. Chem. Soc.* **1973**, *95*, 2803.